JOURNAL OF BACTERIOLOGY, July 2005, p. 4656–4664 Vol. 187, No. 13
0021-9193/05/$08.00+0 doi:10.1128/JB.187.13.4656–4664.2005

Architecture and Adhesive Activity of the *Haemophilus influenzae* Hsf Adhesin

Shane E. Cotter, Hye-Jeong Yeo,† Twyla Juehne, and Joseph W. St. Geme III*

Edward Mallinckrodt Department of Pediatrics and Department of Molecular Microbiology, Washington University School of Medicine, 660 S. Euclid Ave., St. Louis, Missouri 63110

Received 13 January 2005/Accepted 14 March 2005

Haemophilus influenzae **type b is an important cause of meningitis and other serious invasive diseases and initiates infection by colonizing the upper respiratory tract. Among the major adhesins in *H. influenzae* type b is a nonpilus protein called Hsf, a large protein that forms fiber-like structures on the bacterial surface and shares significant sequence similarity with the nontypeable *H. influenzae* Hia autotransporter. In the present study, we characterized the structure and adhesive activity of Hsf. Analysis of the predicted amino acid sequence of Hsf revealed three regions with high-level homology to the HiaBD1 and HiaBD2 binding domains in Hia. Based on examination of glutathione *S*-transferase fusion proteins corresponding to these regions, two of the three had adhesive activity and one was nonadhesive in assays with cultured epithelial cells. Structural modeling demonstrated that only the two regions with adhesive activity harbored an acidic binding pocket like the binding pocket identified in the crystal structure of HiaBD1. Consistent with these results, disruption of the acidic binding pockets in the adhesive regions eliminated adhesive activity. These studies advance our understanding of the architecture of Hsf and the family of trimeric autotransporters and provide insight into the structural determinants of *H. influenzae* type b adherence.**

Haemophilus influenzae is a gram-negative coccobacillus that causes both serious invasive disease and localized respiratory tract disease in humans (26). Isolates of *H. influenzae* can be subdivided into encapsulated and nonencapsulated forms (13). Among encapsulated strains, six structurally and antigenically distinct capsular types exist, designated serotypes a through f (13). Most isolates recovered from patients with invasive disease are encapsulated and express the serotype b capsule, while the majority of strains associated with localized disease are nonencapsulated (nontypeable) (26).

The pathogenesis of *H. influenzae* type b disease begins with colonization of the nasopharynx (26). Most type b strains are capable of expressing hemagglutinating pili, which mediate adherence to mucin, extracellular matrix proteins, and oropharyngeal epithelial cells and facilitate the process of colonization (6, 11, 27). Mutant strains that lack pili are also capable of adherence and colonization, underscoring the importance of nonpilus adhesins (6, 11, 16, 28). Based on in vitro studies with cultured epithelial cells, the major nonpilus adhesin in *H. influenzae* type b is a protein called Hsf (16, 18).

Hsf is a large protein that is encoded by the *hsf* locus and forms fiber-like structures on the bacterial surface (16, 18). In *H. influenzae* type b strain C54, Hsf contains 2,414 amino acids and has a predicted molecular mass of ~245 kDa (18). Southern blot analysis has demonstrated that the *hsf* locus is present in 100% of encapsulated strains tested, including representatives of all six serotypes (18). Interestingly, Hsf shares significant homology with Hia, a 1,098-amino-acid autotransporter protein that is present in ~25% of nontypeable *H. influenzae* strains and mediates efficient attachment to human epithelial cells (3, 17).

The Hia autotransporter contains three functional domains, including an N-terminal signal peptide that targets the protein to the inner membrane, a C-terminal translocator domain that forms a trimer in the outer membrane, and an internal passenger domain that is presented on the bacterial surface via the C-terminal translocator domain (8). The passenger domain of Hia has been shown to possess two distinct binding domains, referred to as HiaBD1 and HiaBD2. These two domains bind to the same host cell receptor, although with differing affinities (10). Based on examination of glutathione *S*-transferase (GST) fusion proteins in assays with Chang epithelial cells, HiaBD1 has a K_d of 0.05 to 0.1 nM and HiaBD2 has a K_d of 1 to 2 nM. In recent work, we solved the crystal structure of HiaBD1 and discovered that the domain is an intricately folded trimer with three identical acidic binding pockets, one on each face of the trimer (29).

In this study, we report that Hsf contains three regions with high-level homology to the binding domains in Hia. Based on assays with GST fusion proteins and Chang epithelial cells, two of the three homologous regions possess adhesive activity and the third is nonadhesive. Structural modeling revealed that only the two regions with adhesive activity harbor an acidic binding pocket like the binding pocket in HiaBD1. Interestingly, disruption of the binding pockets in the two adhesive regions abrogated adhesive activity. These results provide important insights into the mechanism of Hsf-mediated adherence and the determinants of *H. influenzae* type b colonization.

* Corresponding author. Mailing address: Duke University Medical Center, Box 3352, Durham, NC 27710. Phone: (919) 681-4080. Fax: (919) 681-2714. E-mail: j.stgeme@duke.edu.

† Present address: Department of Biochemistry, University of Houston, Houston, Texas.

TABLE 1. Nucleotide primer sequences for generation of pNS1/HsfBD1, pNS1/HsfBD2, and pNS1/HsfBD3

Plasmid	Primers
pNS1/HsfBD1	5′ primer: 5′ GCAGGATCCATTAGCGCGGGTAATAAAG
	3′ primer: 5′ GCAGGTACCTTCATTCGATTTAACCAC
pNS1/HsfBD2	5′ primer: 5′ GCAGTCGACATTAAAGCAGGTAATAAAGC
	3′ primer: 5′ GCAGGATCCTTCAAGACCGCAATCCGC
pNS1/HsfBD3	5′ primer: 5′ GAAGTCGACATTAGTGCGGGTAATAAAGAA
	3′ primer: 5′ GAAGGATCCTTCAAGACCATCACCAACTTTGGC

MATERIALS AND METHODS

Bacterial strains, plasmids, and culture conditions. *Escherichia coli* DH5α (Life Technologies) and *E. coli* BL21(DE3) are laboratory strains that have been described previously (22). Encapsulated *H. influenzae* type b strain C54 is the strain from which *hsf* was originally cloned, and nontypeable *H. influenzae* strain 11 is the strain from which *hia* was originally cloned (3). *H. influenzae* type b strain Eagan is a clinical isolate from a child with meningitis and has been described previously (1).

The plasmid pDC601 contains *hsf* from *H. influenzae* strain C54 cloned into pT7-7, and the plasmid pHMW8-7 contains *hia* from *H. influenzae* strain 11 cloned into pT7-7 (3, 18).

The plasmid pNS1 encodes the Hia signal peptide (amino acids 1 to 49) fused to the Hia translocator domain (amino acids 977 to 1098). To generate this plasmid, first the *hia* promoter and coding sequence for the Hia signal peptide were cloned into the HindIII site in pHAT10 (Clontech). The resulting plasmid was digested with SacI and EcoRI and ligated to a SacI-EcoRI fragment containing coding sequence for the Hia translocator domain. A partial multiple cloning site remained between the coding sequence for the signal peptide and the coding sequence for the translocator domain, allowing insertion of other DNA fragments.

To generate pNS1/HsfBD1, DNA corresponding to residues 1899 to 2032 of Hsf was amplified by PCR from pDC601, engineering BamHI and KpnI sites at the 5′ and 3′ ends, respectively. The resulting fragment was digested with BamHI and KpnI and then ligated into BamHI-KpnI-digested pNS1. To generate pNS1/HsfBD2 and pNS1/HsfBD3, DNA corresponding to Hsf residues 532 to 664 (HsfBD2) and 1209 to 1347 (HsfBD3) was amplified by PCR from pDC601, engineering SalI and BamHI sites at the 5′ and 3′ ends, respectively. The resulting fragments were digested with SalI and BamHI and then ligated into SalI-BamHI-digested pNS1. The primers used to generate pNS1/HsfBD1, pNS1/HsfBD2, and pNS1/HsfBD2 are listed in Table 1.

E. coli strains were grown on Luria-Bertani (LB) agar or in LB broth and were stored at −80°C in LB broth with 30% glycerol. *H. influenzae* was grown on chocolate agar and was stored at −80°C in brain heart infusion broth with 20% glycerol. Plasmids were selected with 100 μg/ml ampicillin.

Recombinant DNA methods. DNA ligations, restriction endonuclease digestions, gel electrophoresis, and PCR were performed according to standard techniques (15). Plasmids were introduced into *E. coli* by electroporation (2).

Site-directed mutagenesis reactions were performed using standard protocols and the QuikChange site-directed mutagenesis kit (Stratagene). Mutagenized plasmids were transformed initially into *E. coli* XL-1 Blue, and nucleotide sequencing was performed. Plasmid clones with the correct nucleotide sequence were then transformed into *E. coli* DH5α or *E. coli* BL21(DE3).

Construction of GST fusion proteins. Constructs for the expression of GST fusion proteins were generated using the vector pGEX-6P-1 (Amersham Pharmacia Biotech). Relevant fragments of DNA were amplified by PCR using primers based on the *hsf* sequence from *H. influenzae* strain C54. Primers were engineered to introduce a BamHI site at the 5′ end of each fragment and a stop codon followed by an EcoRI site at the 3′ end of each fragment. PCR products were digested with BamHI and EcoRI and then ligated into pGEX-6P-1. GST-HsfBD1 encodes Hsf residues 1860 to 2080, GST-HsfBD2 encodes Hsf residues 537 to 738, and GST-HsfBD3 encodes Hsf residues 1169 to 1347.

Purification of GST fusion proteins. In order to purify GST fusion proteins, pGEX-6P-1 derivatives were introduced into *E. coli* BL21(DE3). The resulting strains were grown at 37°C in 250 ml of LB medium containing 100 μg/ml ampicillin to an optical density at 600 nm of ~0.5. Subsequently, isopropyl-β-D-thiogalactopyranoside (IPTG) was added to achieve a final concentration of 0.1 mM, and the cultures were incubated for an additional 5 h at 30°C. Bacteria were harvested by centrifugation at 6,600 × *g* and were then resuspended in 25 ml lysis buffer (5 mM EDTA, 1 mM Pefabloc SC, 1:100 protease inhibitor mix [Roche Molecular Biochemicals] in phosphate-buffered saline [PBS]) and lysed by passing them through a French pressure cell two times. Cell fragments were removed by centrifugation at 10,000 × *g*, Triton X-100 was added to a final concentration of 1%, and GST fusion proteins were isolated by affinity chromatography using glutathione-Sepharose 4B beads (Amersham Pharmacia Biotech). Following extensive washing with PBS, fusion proteins were eluted with elution buffer (25 mM glutathione,100 mM NaCl, 50 mM Tris-HCl, pH 8.0). Alternatively, the Hsf portion was cleaved from GST by adding 80 U/ml PreScission protease (Amersham Pharmacia Biotech) and 1 mM dithiothreitol to the beads and incubating them overnight at 4°C. Isolated proteins were stored in 10% glycerol at −80°C and were analyzed for purity by sodium dodecyl sulfate-polyacrylamide gel electrophoresis and staining with Coomassie blue.

Cell fractionation and protein analysis. Outer membrane proteins were recovered on the basis of Sarkosyl insolubility and were denatured with 95% formic acid as described previously (4, 21). Proteins were then resolved by sodium dodecyl sulfate-polyacrylamide gel electrophoresis and were transferred to nitrocellulose membranes. Western blots were performed with a guinea pig polyclonal antiserum raised against Hsf residues 174 to 608 and a secondary anti-guinea pig immunoglobulin G antiserum conjugated to horseradish peroxidase (Sigma). Proteins were visualized by incubation with a chemiluminescent substrate solution (Pierce) and exposure to film.

Detection of protein binding by immunofluorescence. Chang epithelial cells (Wong-Kilbourne derivative, clone 1-5c-4, human conjunctiva; ATCC CCL20.2) were seeded at a density of 8×10^4 per well onto glass coverslips in 24-well tissue culture plates, and the plates were then incubated overnight. After being washed with PBS, the cells were fixed for 15 min with 2.5% (vol/vol) paraformaldehyde–0.2% (vol/vol) glutaraldehyde in PBS. Subsequently, the monolayers were washed once with PBS and treated with 20 mM ethanolamine in PBS. After being blocked with 3% bovine serum albumin in PBS for 30 min, the cell monolayers were incubated for 1 h with 100 nM of the relevant purified GST fusion protein, and protein binding was detected using an anti-GST antibody (Amersham Pharmacia Biotech; 2 μg/ml) and a Cy2-conjugated secondary antibody (Jackson ImmunoResearch; 1:200). Samples were mounted in Moviol/DABCO and were analyzed by immunofluorescence microscopy.

Quantitation of protein binding by cellular ELISA. ELISAs were performed as described previously (10). Briefly, Chang cells were seeded at a density of 1.8×10^5 per well in 96-well tissue culture plates and were incubated overnight to approximately 90 to 100% confluence. After the monolayers were fixed and nonspecific binding sites were blocked, the relevant protein was added and incubated for 2 h at 37°C. The monolayers were then washed four times with PBS and incubated with an antibody against GST and a horseradish peroxidase-conjugated secondary antibody. Protein binding was quantitated with an ABTS [2,2′-azinobis(3-ethylbenzthiazolinesulfonic acid)] substrate solution (Roche) by measuring absorbance at 405 nm in a microplate reader (Bio-Tek Instruments). K_d values were determined using GraphPad Prism software. Experiments were performed in triplicate on at least three occasions.

Quantitative adherence assays. Adherence assays were performed as described previously (19, 20). Briefly, bacteria were inoculated into broth culture from LB-ampicillin plates and allowed to grow to a density of ~10^9 CFU per ml. Approximately 1×10^7 to 2×10^7 CFU were inoculated onto confluent Chang cell monolayers in 24-well plates, and the plates were centrifuged at 165 × *g* for 5 min. After incubation at 37°C in 5% CO_2 for 25 min, the monolayers were rinsed four times with PBS to remove nonadherent bacteria. Trypsin-EDTA was added to the monolayers, and dilutions were plated on agar to yield the number of adherent CFU per monolayer. Adherence was calculated by dividing the number of adherent CFU per monolayer by the number of inoculated CFU per monolayer.

For adherence inhibition assays, monolayers were preincubated with 100 nM of purified protein, from which the GST moiety had been cleaved, for 1.5 h at 37°C in 5% CO_2. The monolayers were then rinsed twice with PBS to remove unbound protein. At this point, bacteria were inoculated, and adherence was measured as described above.

Sequencing of the *hsf* gene from *H. influenzae* strain Eagan. The *hsf* gene from *H. influenzae* strain Eagan was amplified by PCR using genomic DNA as a template and platinum *Pfx* polymerase (Invitrogen). PCR primers were constructed corresponding to the regions just 5′ and 3′ to the coding region of strain C54 *hsf*, with engineered EcoRI and BamHI sites, respectively. The resulting

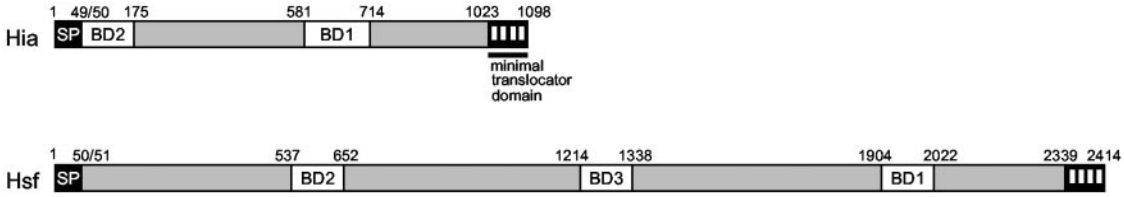

FIG. 1. Schematic representation of Hsf similarity to Hia in regions of functional significance. The signal peptide of each protein is depicted in black and labeled SP. The Hia minimal translocation domain is represented in black with white stripes. The two binding domains of Hia are represented as white boxes and are labeled BD1 and BD2, respectively. The amino acid residues defining the boundaries of these regions are listed above each of them. The C terminus of Hsf is represented in black with white stripes to indicate its absolute identity to the Hia minimal translocator domain. Three regions of Hsf share homology with the Hia binding domains and are represented with white boxes. These have been labeled BD1, BD2, and BD3.

product was gel purified, digested, and ligated into EcoRI-BamHI-digested pT7-7. The entire insert was then sequenced with 2× coverage and assembled using the ContigExpress program (Vector NTI).

Nucleotide sequencing and DNA and protein sequence analyses. Nucleotide sequencing was performed using an ABI automated sequencer and the Big Dye Terminator Premix-20 kit version 3.1 (Applied Biosystems–Perkin-Elmer), with double-stranded plasmid DNA as a template. DNA sequence analysis was performed using the Genetics Computer Group software package from the University of Wisconsin (Wisconsin Package version 10; Genetics Computer Group, Madison, WI). Amino acid sequence alignments were performed using BLAST at the National Center for Biotechnology Information (http://www.ncbi.nlm.nih.gov/BLAST/) and ClustalW at EBI (http://www.ebi.ac.uk/clustalw/).

Sequence alignments and molecular modeling. The amino acid sequence of the HiaBD1 binding domain (Hia residues 586 to 705) was aligned with the homologous sequences in Hsf (HsfBD1, residues 1904 to 2022; HsfBD2, residues 537 to 653; and HsfBD3, residues 1214 to 1338). The pairwise sequence alignments of HiaBD1-HsfBD1, HiaBD1-HsfBD2, and HiaBD1-HsfBD3 were generated using the ClustalW program and SWISS-MODEL (Automated Protein Modeling Server) (7, 25). The basic pairwise alignment of each set is identical to the multiple sequence alignment of HiaBD1. Homology models of the HsfBD1, HsfBD2, and HsfBD3 subunits were built using the MODELER module available in the INSIGHTII software (Accelrys Inc., San Diego, CA) and on the SWISS-MODEL server. To generate homotrimers, the structures of the three subunits were superimposed onto the crystal structure of the HiaBD1 trimer using graphic program O (9). The final models generated after energy minimization were evaluated for stereochemical quality using the validation program PROCHECK. Ramachandran plots of the model structures indicated that over 96% of residues were in allowed regions, with no disallowed regions.

Nucleotide sequence accession number. The accession number for the strain Eagan *hsf* gene sequence is AY823627.

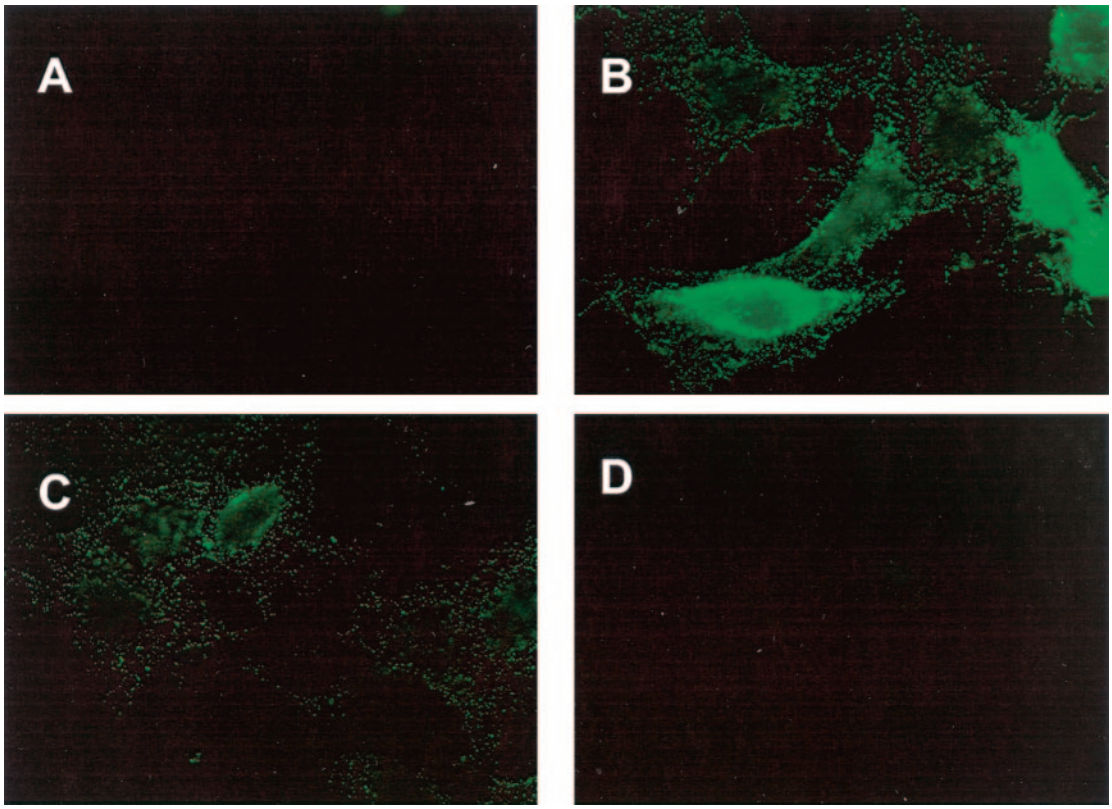

FIG. 2. Binding by GST-Hsf fusion proteins to Chang epithelial cells, assessed by immunofluorescence microscopy. GST alone (A), GST-HsfBD1 (B), GST-HsfBD2 (C), and GST-HsfBD3 (D) were incubated with fixed Chang epithelial cells for 90 min. After the cells were washed, bound protein was visualized using an antiserum against GST and a Cy2-conjugated secondary antibody. Exposure times were identical for all samples.

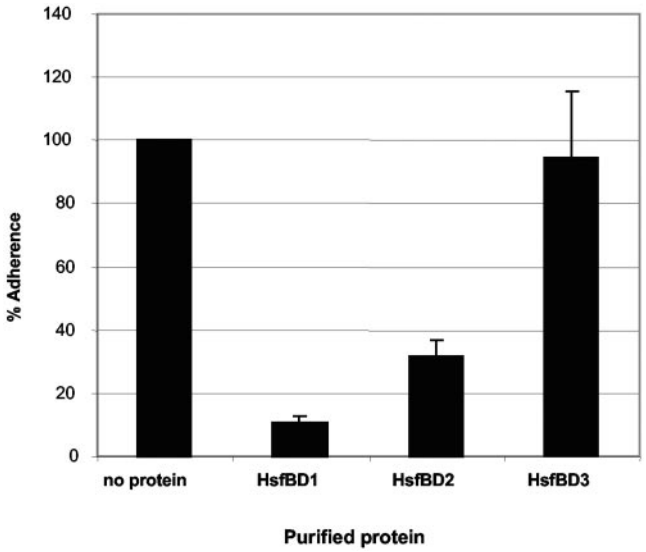

FIG. 3. Inhibition of Hsf-mediated bacterial adherence by purified HsfBD1, HsfBD2, and HsfBD3. Chang epithelial cells were preincubated for 90 min with 100 nM of purified HsfBD1, HsfBD2, or HsfBD3. After the cells were washed to remove unbound protein, ~1.5 $\times$ 10^7 CFU of BL21(DE3)/pDC601, expressing full-length Hsf, were inoculated onto the monolayers, and adherence was measured in a standard 30-minute adherence assay. Adherence values were normalized to adherence by BL21(DE3)/pDC601 to monolayers that were not pretreated with purified protein (no protein; defined as 100%). The absolute level of adherence by BL21(DE3)/pDC601 by itself was approximately 10^7 CFU per monolayer. The bars represent means plus standard errors of three measurements from a representative experiment.

RESULTS

Hsf has a conserved architecture and high similarity to Hia in regions of functional significance. In earlier work, we focused on the Hsf protein expressed by *H. influenzae* type b strain C54. To expand our understanding of the functional domains of Hsf, we began by cloning and sequencing the *hsf* gene from *H. influenzae* strain Eagan, a serotype b strain that belongs to one of the two most common clonal groups implicated in invasive disease (12). The resulting gene was found to contain 7,242 nucleotides, encoding a protein with 2,414 amino acids and a predicted molecular mass of ~245 kDa. The predicted amino acid sequence of Hsf_{Eagan} is virtually identical to the predicted sequence of Hsf_{C54}, with only four divergent amino acids.

As shown schematically in Fig. 1, comparison of the amino acid sequences of Hsf_{C54}, Hsf_{Eagan}, and Hia_{11} revealed several notable features. In particular, the Hsf and Hia proteins share absolute identity over the final 76 amino acids, a region found previously to represent the minimal translocator domain in Hia (necessary for presentation of the Hia passenger domain on the bacterial surface) (24). In addition, residues 1904 to 2022 at the C-terminal end of Hsf share 71% identity and 89% similarity with the HiaBD1 domain and 44% identity and 80% similarity with the HiaBD2 domain, residues 537 to 652 near the N-terminal end of Hsf share 49% identity and 87% similarity with HiaBD1 and 63% identity and 89% similarity with HiaBD2, and residues 1214 to 1338 in the middle of Hsf share 41% identity and 73% similarity with HiaBD1 and 35% identity and 69% similarity with HiaBD2. Based on the relative levels of homology to HiaBD1 and HiaBD2, we refer to these regions as HsfBD1 (residues 1904 to 2022), HsfBD2 (residues 537 to 652), and HsfBD3 (residues1214 to 1338), respectively.

Hsf contains two binding pockets with differing binding affinities. Given the homology between HsfBD1, HsfBD2, and HsfBD3 and the HiaBD1 and HiaBD2 binding domains, we examined the adhesive activities of the HsfBD1, HsfBD2, and HsfBD3 regions in assays with Chang conjunctival cells. As a first step, we generated GST fusion proteins containing HsfBD1 (GST-HsfBD1), HsfBD2 (GST-HsfBD2), and HsfBD3 (GST-HsfBD3). Following purification of these proteins, 100 nM quantities were incubated with epithelial cell monolayers, and binding was assessed by immunofluorescence microscopy using an antiserum against GST and a Cy2 secondary antibody. As shown in Fig. 2, GST-HsfBD1 demonstrated strong punctate fluorescence, GST-HsfBD2 demonstrated low-intensity punctate fluorescence, and GST-HsfBD3 demonstrated only background fluorescence (indistinguishable from GST alone).

To extend these results, we examined the ability of 100 nM of the purified fusion proteins to inhibit adherence by *E. coli* expressing wild-type Hsf. As shown in Fig. 3, preincubation of Chang epithelial cell monolayers with HsfBD1 almost completely blocked bacterial Hsf-mediated adherence. In contrast, preincubation with HsfBD2 resulted in only a partial block of adherence, and preincubation with HsfBD3 had no effect on adherence, consistent with our findings using immunofluorescence microscopy.

Given the differences in adhesive activity of the HsfBD1 and HsfBD2 regions as assessed by immunofluorescence micros-

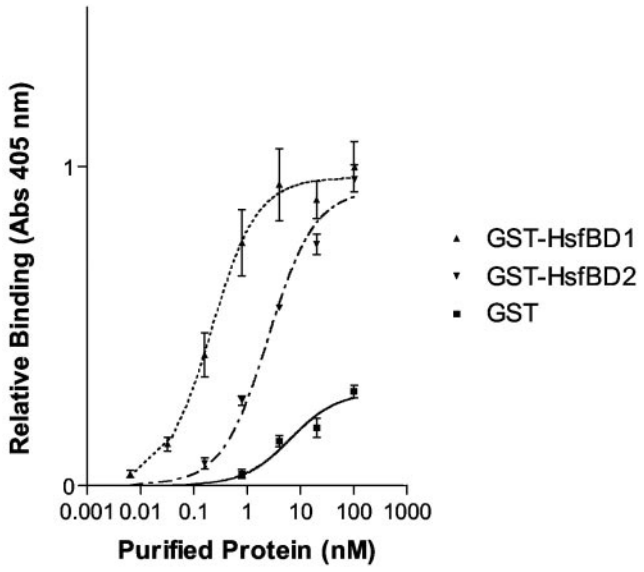

FIG. 4. Determination of relative binding of the functional Hsf binding domains. GST-HsfBD1, GST-HsfBD2, and GST alone were added to Chang epithelial cell monolayers and incubated for 2 h. After unbound protein was washed off, binding was measured by ELISA using an antibody against GST and a horseradish peroxidase-conjugated secondary antibody. Abs, absorbance. The error bars indicate standard deviations.

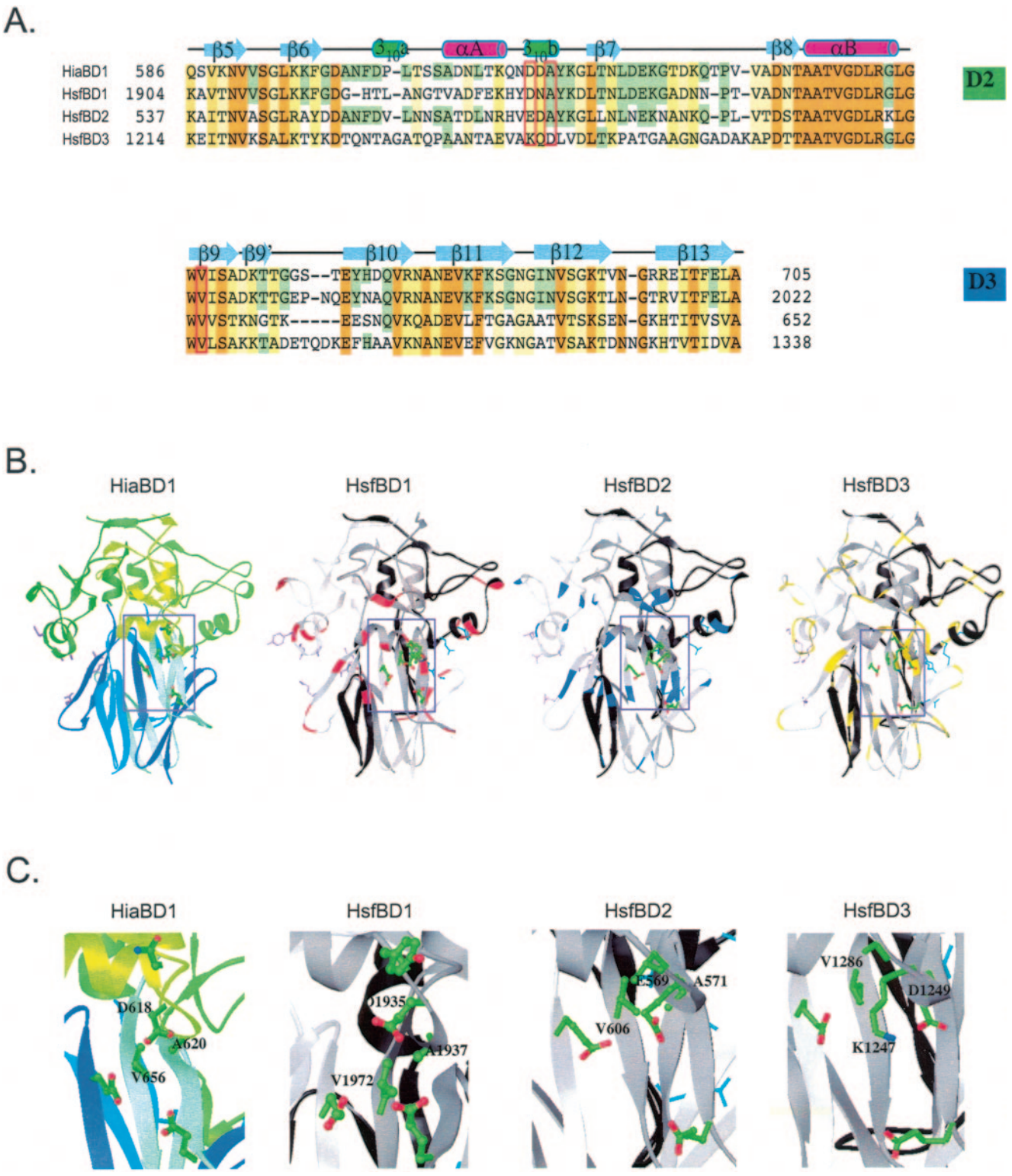

FIG. 5. Homology modeling of the Hsf binding domains. (A) Sequence alignment of HiaBD1 (residues 586 to 705) with homologous regions in Hsf. Residues that are identical in all sequences are highlighted in orange, and residues that are conserved in all sequences are highlighted in yellow. Residues that are identical to the HiaBD1 sequence are indicated with green boxes. Essential amino acids in the binding pocket of HiaBD1 are indicated with red boxes. The previously annotated secondary structural elements of HiaBD1 are shown at the top of the sequence alignment, with β strands and helices indicated as arrows and cylinders, respectively. D2 and D3 indicate domain 2 and domain 3 of HiaBD1. (B) Ribbon diagrams of crystal structure of HiaBD1 and homology-modeled structures of HsfBD1, HsfBD2, and HsfBD3. Domain 2 and domain 3 (defined in panel A) of HiaBD1 are colored in green and blue, respectively. Each subunit of the HiaBD1 trimer is colored in a different shade of green or blue. In the modeled structures of HsfBD1, HsfBD2, and HsfBD3, the subunits of the trimer are colored in silver, gray, and black, and nonconserved residues between HiaBD1 and HsfBD1, between HiaBD1 and HsfBD2, and between HiaBD1 and HiaBD2 are color coded in red, blue, and yellow, respectively. Previously identified active-site residues in HiaBD1 and corresponding residues in HsfBD1, HsfBD2, and HsfBD3 are shown in ball-and-stick representation. (C) Close-up views of the active sites in HiaBD1, HsfBD1, HsfBD2, and HsfBD3. Residues are in ball-and-stick representation and color-coded green for carbon, red for oxygen, and blue for nitrogen.

copy and adherence inhibition, we evaluated binding affinities using a cell-based ELISA. GST fusion proteins were added to Chang epithelial cell monolayers in 96-well plates at concentrations ranging from 6 pM to 100 nM, and binding was detected using anti-GST antiserum. As shown in Fig. 4, GST-HsfBD1 bound with high affinity, with a K_d of ~0.2 nM. GST-HsfBD2 bound with significantly lower affinity, with a K_d of ~2.5 nM. This ~10-fold difference in affinity was observed in multiple experiments and is similar to the difference detected between HiaBD1 and HiaBD2 in Hia (10).

Homology modeling of HsfBD1, HsfBD2, and HsfBD3. To begin to elucidate why HsfBD1 and HsfBD2 are adhesive and HsfBD3 is nonadhesive, we generated model structures of the three domains, using the crystal structure of HiaBD1 (PDB code, 1S7 M), which was solved at 2.1 Å. In previous work, we demonstrated that domains D2 and D3 of each subunit of HiaBD1 (D2 and D3 in Fig. 5A) form an acidic binding pocket, resulting in three independent binding sites on the surface of the HiaBD1 trimer. The core of the acidic binding pocket is defined by HiaBD1 residues D618, A620, and V656. As shown in the multiple sequence alignment depicted in Fig. 5A, the secondary structural elements observed in HiaBD1 are well conserved in HsfBD1, HsfBD2, and HsfBD3. In addition, the crystal structure of HiaBD1 and the model structures of HsfBD1, HsfBD2, and HsfBD3 possess the same fold and trimer assembly (Fig. 5B). The HiaBD1 structure and the HsfBD1 structure are most similar, and the residues essential for HiaBD1 binding activity (D618, A620, and V656) are strictly conserved in the HsfBD1 model structure (D1935, A1937, and V1972), creating an analogous binding pocket. The residues essential for HiaBD1 binding activity are also conserved in the HsfBD2 model structure (E569, A571, and V606), again creating an analogous binding pocket. In contrast, the HsfBD3 model structure lacks an acidic binding pocket, containing K1247 and D1249 at the residues that correspond to D618 and A620 in HiaBD1. Closer examination revealed that the basic K1247 residue in HsfBD3 spans the pocket and creates a surface that differs significantly from the acidic binding pocket in HiaBD1.

HsfBD1 and HsfBD2 mediate adherence to epithelial cells via an acidic pocket similar to the pocket in HiaBD1. To validate the HsfBD1, HsfBD2, and HsfBD3 model structures and establish the structural determinants of Hsf adhesive activity, we began by expressing HsfBD1, HsfBD2, or HsfBD3 individually on the surface of *E. coli*. Our approach involved generation of chimeric proteins with HsfBD1, HsfBD2, or HsfBD3 inserted between the Hia signal peptide (amino acids 1 to 49) and the Hia translocator domain (amino acids 977 to 1098), allowing surface presentation of the relevant Hsf domain. Western analysis of the resulting *E. coli* strains established that the chimeric proteins were localized in the outer membrane in comparable amounts (data not shown). As shown in Fig. 6, *E. coli*/HsfBD1 and *E. coli*/HsfBD2 exhibited high-level adherence to cultured epithelial cells, while *E. coli*/HsfBD3 was nonadherent.

To assess the importance of the acidic pockets in HsfBD1 and HsfBD2, we mutated D1935 in the HsfBD1 chimeric protein and E569 in the HsfBD2 chimeric protein to alanine residues. Examination of outer membrane fractions from the resulting recombinant strains revealed that the mutated proteins were localized to the outer membrane and were present at wild-type levels (data not shown). Similar to previous observations with the D618A mutation in HiaBD1, mutation of D1935 and E569 completely eliminated adhesive activity (Fig. 6) in assays with Chang epithelial cells, arguing that HiaBD1, HsfBD1, and HsfBD2 bind to epithelial cells via a common acidic patch.

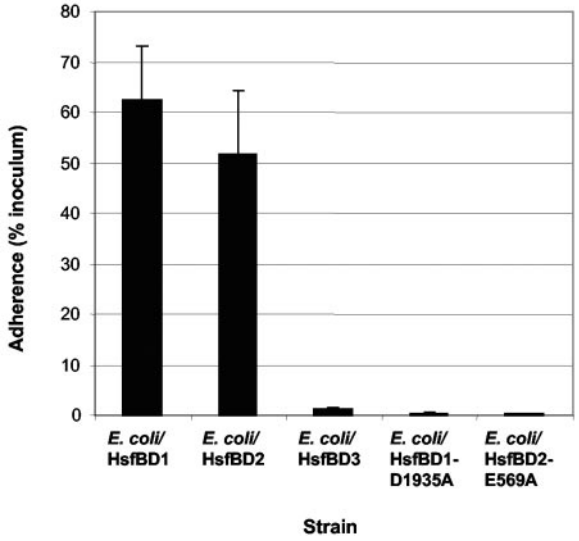

FIG. 6. Adherence by Hsf binding domains expressed individually as chimeric proteins in *E. coli* strain DH5α. DH5α/HsfBD1, DH5α/HsfBD2, and DH5α/HsfBD3 were inoculated onto Chang epithelial cell monolayers and incubated for 30 min at 37°C. After the monolayers were rinsed to remove unbound bacteria, adherent bacteria were quantitated. Adherence is plotted as a percentage of the bacterial inoculum that bound to the epithelial cell monolayer. HsfBD1-D1936A is identical to HsfBD1 except that it contains an aspartic acid-to-alanine mutation at residue 1936. HsfBD2-E569A is equivalent to HsfBD2 except that it contains a glutamic acid-to-alanine mutation at residue 569. The error bars indicate standard deviations.

To examine the interrelationship between the HsfBD1 and HsfBD2 binding domains, we introduced the E569A and the D1935A point mutations individually and in combination in full-length Hsf and then expressed the resulting proteins in *E. coli*. As shown in Fig. 7A, the point mutations had no effect on the amount of Hsf present in the bacterial outer membrane. Consistent with the high-level adherence mediated by the HsfBD1 and HsfBD2 domains in isolation, neither the E569A mutation by itself nor the D1935A mutation by itself had any effect on adherence (Fig. 7B). However, the E569A and the D1935A mutations in combination completely eliminated Hsf-mediated adherence (Fig. 7B).

Considered together, these findings indicate that HsfBD1 and HsfBD2 contribute independently to Hsf-mediated adherence to Chang epithelial cells and provide further evidence that HsfBD3 lacks adhesive activity.

DISCUSSION

In this study, we examined the architecture and adhesive activity of the *H. influenzae* type b Hsf adhesin. Alignment of the predicted amino acid sequences of Hsf proteins from two different type b strains and the Hia protein from a prototype

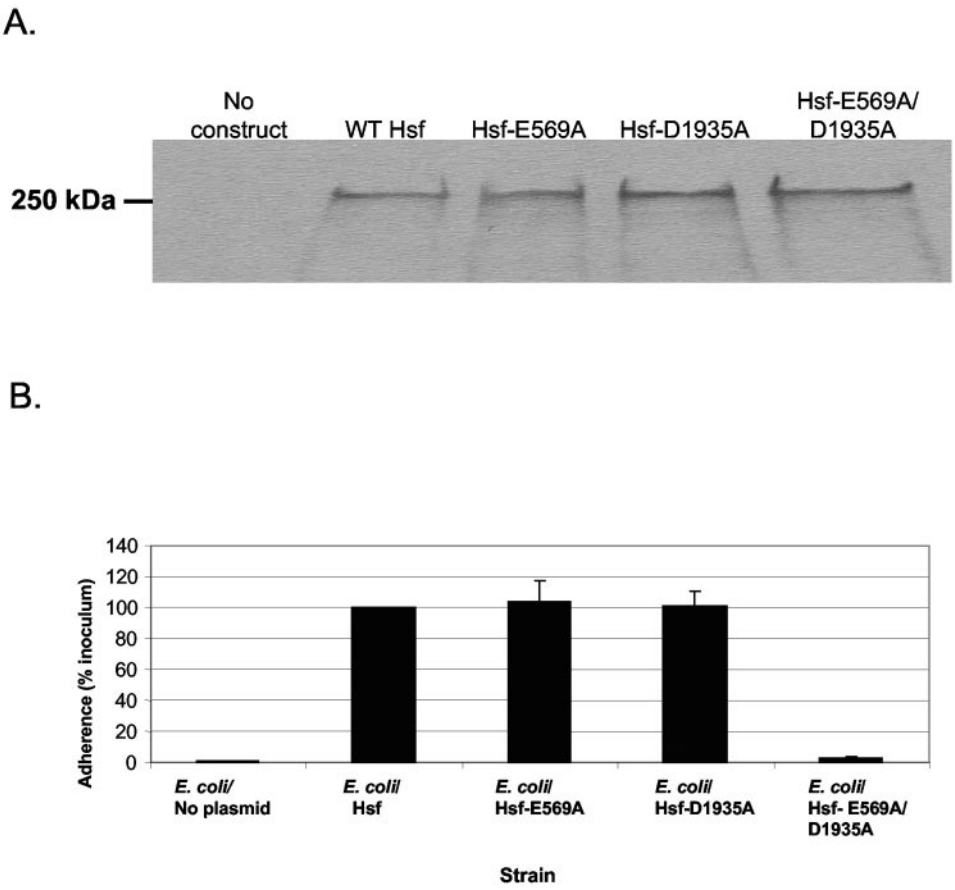

FIG. 7. Effects of binding domain point mutations on bacterial adherence mediated by full-length Hsf. (A) Outer membrane fractions were isolated from *E. coli* BL21(DE3) expressing wild-type or mutant Hsf, and Hsf was detected by Western analysis. (B) Adherence to Chang epithelial cell monolayers by *E. coli* BL21(DE3) expressing wild-type or mutant Hsf was measured in quantitative assays. Adherence values were normalized to adherence by BL21(DE3) expressing wild-type Hsf, defined as 100%. The bars represent means plus standard errors of three measurements from a representative experiment.

nontypeable strain revealed absolute identity over the C-terminal 76 amino acids. In earlier work on Hia, we established that this region harbors translocator activity and defines the subfamily of trimeric autotransporters (24, 29). Accordingly, we conclude that Hsf is a trimeric autotransporter protein.

Upon closer examination of the alignment of Hsf and Hia sequences, we observed that three distinct regions in the Hsf passenger domain share striking homology with the HiaBD1 and HiaBD2 binding domains in Hia. Further analysis established that two of the three homologous regions harbor adhesive activity and possess an acidic binding pocket like the binding pocket identified in the crystal structure of HiaBD1. Based on experiments using purified protein, these two regions have distinct binding affinities that differ by approximately 10-fold, analogous to the HiaBD1 and HiaBD2 binding domains. As with Hia, the higher-affinity Hsf adhesive region (HsfBD1) is located near the C terminus of the passenger domain and the lower-affinity adhesive region (HsfBD2) is located near the N terminus of the passenger domain. In this context, it is interesting that the higher-affinity Hsf adhesive region is most similar to HiaBD1 and the lower-affinity Hsf adhesive region is most similar to HiaBD2, based on comparison of primary amino acid sequences.

Given that Hsf is anchored in the outer membrane by its C-terminal translocator domain and forms a fiber on the bacterial surface, it is likely that HsfBD2 is situated away from the bacterial cell wall, at the distal end of the fiber. This arrangement raises the possibility that Hsf-mediated adherence to host cells is a two-step process that exploits the different binding affinities of HsfBD1 and HsfBD2. In particular, the lower-affinity HsfBD2 domain may make initial contact with the host cell and may then be displaced by the higher-affinity HsfBD1 domain, resulting in a ratcheting effect that pulls the bacterium closer to the host cell surface. This ratcheting effect may be especially important in an encapsulated organism, where the polysaccharide capsule may mask HsfBD1 and make it relatively inaccessible to the host cell. According to this model, the lower-affinity binding domain must be responsible for the initial interaction with the receptor and hence must be located at the distal end of the Hsf fiber, allowing competitive displacement by the higher-affinity binding domain. If instead the higher-affinity binding domain were located at the tip of the fiber and responsible for initial contact, competitive displacement would not occur and intimate adherence would be hindered.

As another model for Hsf-mediated interaction with host cells, it is possible that HsfBD1 and HsfBD2 engage in a

bivalent interaction independent of their relative locations within the Hsf fiber. The HsfBD1 and HsfBD2 binding domains in a single Hsf fiber may bind to two separate receptor molecules or to homologous domains on the same receptor, increasing the avidity of the interaction with the host cell surface and stabilizing adherence despite significant physical forces in the respiratory tract, including the mucociliary escalator, coughing, and sneezing. Of note, there are several eukaryotic cell adhesion molecules that mediate cell-cell contact via multiple binding domains and multivalent interactions with the same target molecule. Examples include neural cell adhesion molecule, PECAM-1, and cadherins (5, 14, 23).

We found that HsfBD1 and HsfBD2 demonstrated different binding affinities when assessed by ELISA using purified GST fusion proteins but mediated similar levels of bacterial adherence when expressed on the surfaces of bacteria either as chimeric proteins or in the context of full-length Hsf. In considering this apparent inconsistency, we propose that the presence of multiple subunits on the surface of a single bacterium provides a compensatory effect that allows proteins with decreased affinity to mediate full-level adherence within our assay. Indeed, previous experiments mapping the adhesive pocket within HiaBD1 support this point. In particular, isolated mutations of N617, E668, and E678 resulted in a marked decrease in the adhesive function of GST-HiaBD1 but had no effect on adherence when present in Hia expressed on the surfaces of bacterial cells (29). Of note, our in vitro adherence assay lacks the shear forces and other variables present during natural infection, potentially precluding appreciation of the different affinities of HsfBD1 and HsfBD2.

The overall similarities between the HiaBD1 crystal structure and the HsfBD1 and HsfBD2 model structures raised the possibility that these domains interact with epithelial cells by a conserved mechanism. Consistent with this possibility, the acidic binding pocket in HiaBD1 is present in HsfBD1 and HsfBD2 as well. Furthermore, individual point mutations disrupting this pocket in HsfBD1 and HsfBD2 completely abrogated the adhesive function. Considered together, these observations argue strongly that Hia and Hsf interact with the same host cell receptor and that encapsulated and nonencapsulated strains of *H. influenzae* may compete with each other for adhesive surfaces in the respiratory tract. With this information in mind, it is likely that compounds designed to prevent Hsf-mediated colonization by encapsulated *H. influenzae* would also block colonization by a significant fraction of nontypeable *H. influenzae* strains.

In Hsf, the sequence between the HsfBD1 and HsfBD2 binding domains is 1,252 amino acids in length, approximately three times longer than the sequence between the HiaBD1 and HiaBD2 binding domains in Hia (406 amino acids). The length of the intervening sequence in Hsf may be critical to extend HsfBD2 beyond the polysaccharide capsule and allow adherence in the presence of encapsulation. Interestingly, the intervening sequence in Hsf contains the HsfBD3 domain, which shares significant homology with HiaBD1 but lacks the acidic binding pocket critical for adhesive activity in HiaBD1, HsfBD1, and HsfBD2. Closer examination of the alignment of HsfBD3 and HiaBD1 reveals that sequence homology is highest over the C-terminal halves of the sequences, corresponding to the region designated domain 3 in HiaBD1. Domain 3 contains extensive interdigitation of β strands from the three subunits in the trimer and is believed to play an important role in stabilizing the trimeric structure (29). Accordingly, it is possible that HsfBD3 evolved to serve a structural role, stabilizing the long intervening sequence in Hsf and facilitating accessibility of HsfBD2 to host cell receptors. It is also possible that HsfBD3 mediates adherence to different cell types by a different mechanism, independent of an acidic binding pocket.

In summary, our results establish that the *H. influenzae* type b Hsf adhesin has two binding domains, namely, the HsfBD1 domain located adjacent to the bacterial cell wall and the HsfBD2 domain, which appears to be located near the tip of the Hsf fiber. Both HsfBD1 and HsfBD2 share significant homology with the HiaBD1 high-affinity binding domain in Hia and mediate adherence via a conserved acidic binding pocket. The HsfBD3 domain also shares similarity with HiaBD1 but lacks the acidic binding pocket and lacks adhesive activity in assays with Chang epithelial cells. We propose that HsfBD3 may play an important structural role, stabilizing the Hsf fiber and facilitating Hsf-mediated adherence in the context of a polysaccharide capsule.

ACKNOWLEDGMENTS

We thank S. Laarmann and N. Surana for useful discussions.

This work was supported by U.S. Public Health Service Grant RO1-AI44167 to J.W.S. and by U.S. Public Health Service Training Grant T32-HL07873 to S.E.C. S.E.C. is a member of the Medical Scientist Training Program at Washington University School of Medicine.

REFERENCES

1. **Anderson, P., R. B. Johnston, Jr., and D. H. Smith.** 1972. Human serum activity against *Haemophilus influenzae* type b. J. Clin. Investig. **51:**31–38.
2. **Ausubel, F. M., R. Brent, R. E. Kingston, D. D. Moore, J. G. Seidman, J. A. Smith, and K. Struhl.** 1994. Current protocols in molecular biology. John Wiley & Sons, New York, N.Y.
3. **Barenkamp, S. J., and J. W. St. Geme III.** 1996. Identification of a second family of high-molecular-weight adhesion proteins expressed by non-typable *Haemophilus influenzae*. Mol. Microbiol. **19:**1215–1223.
4. **Carlone, G. M., M. L. Thomas, H. S. Rumschlag, and F. O. Sottnek.** 1986. Rapid microprocedure for isolating detergent-insoluble outer membrane proteins from *Haemophilus* species. J. Clin. Microbiol. **24:**330–332.
5. **Chappuis-Flament, S., E. Wong, L. D. Hicks, C. M. Kay, and B. M. Gumbiner.** 2001. Multiple cadherin extracellular repeats mediate homophilic binding and adhesion. J. Cell Biol. **154:**231–243.
6. **Farley, M. M., D. S. Stephens, S. L. Kaplan, and E. O. Mason.** 1990. Pilus- and non-pilus-mediated interactions of *Haemophilus influenzae* type b with human erythrocytes and human nasopharyngeal mucosa. J. Infect. Dis. **154:** 752–759.
7. **Guex, N., and M. C. Peitsch.** 1997. SWISS-MODEL and the Swiss-PdbViewer: an environment for comparative protein modeling. Electrophoresis **18:**2714–2723.
8. **Henderson, I. R., F. Navarro-Garcia, and J. P. Nataro.** 1998. The great escape: structure and function of the autotransporter proteins. Trends Microbiol. **6:**370–378.
9. **Jones, T. A., J. Y. Zou, S. W. Cowan, and Kjeldgaard.** 1991. Improved methods for building protein models in electron density maps and the location of errors in these models. Acta Crystallogr. A **47:**110–119.
10. **Laarmann, S., D. Cutter, T. Juehne, S. J. Barenkamp, and J. W. St. Geme III.** 2002. The *Haemophilus influenzae* Hia autotransporter harbours two adhesive pockets that reside in the passenger domain and recognize the same host cell receptor. Mol. Microbiol. **46:**731–743.
11. **Loeb, M. R., E. Connor, and D. Penney.** 1988. A comparison of the adherence of fimbriated and nonfimbriated *Haemophilus influenzae* type b to human adenoids in organ culture. Infect. Immun. **49:**484–489.
12. **Musser, J. M., J. S. Kroll, D. M. Granoff, E. R. Moxon, B. R. Brodeur, J. Campos, H. Dabernat, W. Frederiksen, J. Hamel, G. Hammond, et al.** 1990. Global genetic structure and molecular epidemiology of encapsulated *Haemophilus influenzae*. Rev. Infect. Dis. **12:**75–111.
13. **Pittman, M.** 1931. Variation and type specificity in the bacterial species *Haemophilus influenzae*. J. Exp. Med. **53:**471–493.
14. **Ranheim, T. S., G. M. Edelman, and B. A. Cunningham.** 1996. Homophilic adhesion mediated by the neural cell adhesion molecule involves multiple immunoglobulin domains. Proc. Natl. Acad. Sci. USA **93:**4071–4075.

15. **Sambrook, J., and D. W. Russel.** 2001. Molecular cloning: a laboratory manual, 4th ed. Cold Spring Harbor Laboratory Press, Cold Spring Harbor, N.Y.
16. **St. Geme, J. W., III, and D. Cutter.** 1995. Evidence that surface fibrils expressed by *Haemophilus influenzae* type b promote attachment to human epithelial cells. Mol. Microbiol. **15:**77–85.
17. **St. Geme, J. W., III, and D. Cutter.** 2000. The *Haemophilus influenzae* Hia adhesin is an autotransporter protein that remains uncleaved at the C terminus and fully cell associated. J. Bacteriol. **182:**6005–6013.
18. **St. Geme, J. W., III, D. Cutter, and S. J. Barenkamp.** 1996. Characterization of the genetic locus encoding *Haemophilus influenzae* type b surface fibrils. J. Bacteriol. **178:**6281–6287.
19. **St. Geme, J. W., III, and S. Falkow.** 1990. *Haemophilus influenzae* adheres to and enters cultured human epithelial cells. Infect. Immun. **58:**4036–4044.
20. **St. Geme, J. W., III, S. Falkow, and S. J. Barenkamp.** 1993. High-molecular-weight proteins of nontypable *Haemophilus influenzae* mediate attachment to human epithelial cells. Proc. Natl. Acad. Sci. USA **90:**2875–2879.
21. **St. Geme, J. W., III, V. V. Kumar, D. Cutter, and S. J. Barenkamp.** 1998. Prevalence and distribution of the *hmw* and *hia* genes and the HMW and Hia adhesins among genetically diverse strains of nontypeable *Haemophilus influenzae*. Infect. Immun. **66:**364–368.
22. **Studier, F. W., and B. A. Moffatt.** 1986. Use of bacteriophage T7 RNA polymerase to direct high-level expression of cloned genes. J. Mol. Biol. **189:**113–130.
23. **Sun, Q. H., H. M. DeLisser, M. M. Zukowski, C. Paddock, S. M. Albelda, and P. J. Newman.** 1996. Individually distinct Ig homology domains in PECAM-1 regulate homophilic binding and modulate receptor affinity. J. Biol. Chem. **271:**11090–11098.
24. **Surana, N. K., D. Cutter, S. J. Barenkamp, and J. W. St. Geme III.** 2004. The *Haemophilus influenzae* Hia autotransporter contains an unusually short trimeric translocator domain. J. Biol. Chem. **279:**14679–14685.
25. **Thompson, J. D., D. G. Higgins, and T. J. Gibson.** 1994. CLUSTAL W: improving the sensitivity of progressive multiple sequence alignment through sequence weighting, position-specific gap penalties and weight matrix choice. Nucleic Acids Res. **22:**4673–4680.
26. **Turk, D. C.** 1984. The pathogenicity of *Haemophilus influenzae*. J. Med. Microbiol. **18:**1–16.
27. **Virkola, R., M. Brummer, H. Rauvala, L. van Alphen, and T. K. Korhonen.** 2000. Interaction of fimbriae of *Haemophilus influenzae* type B with heparin-binding extracellular matrix proteins. Infect. Immun. **68:**5696–5701.
28. **Weber, A., K. Harris, S. Lohrke, L. Forney, and A. L. Smith.** 1991. Inability to express fimbriae results in impaired ability of *Haemophilus influenzae* b to colonize the nasopharynx. Infect. Immun. **59:**4724–4728.
29. **Yeo, H. J., S. E. Cotter, S. Laarmann, T. Juehne, J. W. St. Geme, and G. Waksman.** 2004. Structural basis for host recognition by the *Haemophilus influenzae* Hia autotransporter. EMBO J. **23:**1245–1256.